

Polarization independent parametric upconversion for vector light

Hai-Jun Wu,¹ Bo Zhao,¹ Carmelo Rosales-Guzmán,¹ Wei Gao,¹ Bao-Sen Shi,^{1,2} and Zhi-Han Zhu^{1,*}

¹Wang Da-Heng Collaborative Innovation Center, Heilongjiang Provincial Key Laboratory of Quantum Manipulation & Control, Harbin University of Science and Technology, Harbin 150080, China

²CAS Key Laboratory of Quantum Information, University of Science and Technology of China, Hefei, 230026, China

Frequency conversion of vectorially structured light, without altering the spin-orbit coupling (SOC) state of the signal light, is crucial for frontier optical research based on structured light, however, realizing such conversion remains a challenge. In this proof-of-principle work, we demonstrated polarization independent parametric upconversion using a polarization Sagnac nonlinear interferometer based on type-II second-harmonic generation (SHG). Our results demonstrate that the vector (including both polarization and intensity) profile and associated SOC state of the signal vector beam could be transferred to the SHG output with a high fidelity. This work lays a foundation for vector full-field quantum frequency conversion and also paves the way for upconversion detection for polarization-resolved imaging and microscopy.

Introduction. — A light field’s state of polarization (SoP) deterministically describes its spin nature, and the field is broadly referred to as vector light (or vectorially structured light) when the SoP is spatially non-uniform [1–3]. The feature of carrying a spatially-variant SoP indicates that there is subwavelength inhomogeneity within the photons, which originates from photonic spin-orbit coupling (SOC); hence the spatially-variant SoP can be described as SOC state [4–6]. Historically, vector light has been discovered soon after the invention of the laser [7,8]; however, it was not until much later ago that researchers revealed its unique focusing properties and the SOC nature [9,10]. Thereafter, it has been widely studied and resulted in a number of innovations throughout the main fields of modern optics, such as imaging, optical trapping, communication and fundamental physics [11–19]. In this new subfield of modern optics, the ability for on-demand shaping of vector light is crucial for both fundamental and application aspects. For the task, a straightforward approach is manipulation of the Geometric phase via planar optical elements with artificial microstructure [5,6]. Additionally, another promising approach is using nonlinear optical interactions with vector light; here, one can simultaneously manipulate the multiple degrees of freedom (DoFs) of light, including the frequency, amplitude and angular momenta. In particular, the SOC-mediated nonlinear polarization afforded by vector nonlinear optics, as an additional auxiliary interface, can significantly enhance our ability to shape and control nonlinear interactions. For this, recently, this topic has raised considerable interest in the community of nonlinear optics, ranging from second-harmonic generation (SHG) and stimulated Brillouin/Raman scattering to high-order harmonic generation [20–30].

Among the various nonlinear applications, optical parametric conversion based on second-order interactions, as a frequency converter, is the most basic but also the most important one presently used in laser and photonic systems.

Such a basic function, however, is not easy to accomplish when it meets a vector light. Because it is difficult for currently available nonlinear crystals to convert orthogonally-polarized components of the light simultaneously. A feasible solution would be the use of nonlinear interferometers with SU(2) symmetry [31], for which the two-crystal and Sagnac schemes (both are phase-locking structure) are two reliable configurations that have already become standard methods for the generation of polarization entanglement [32–34]. Several groups have recently demonstrated the SHG of vector light via a two-crystal scheme consisting of orthogonal thin type-I crystals [35,36]. It should be noted that while long periodically poled crystals are high efficiency, they are not easy to devise in the two-crystal scheme because they introduce a Rayleigh-distance shift between the orthogonal polarization components of the SHG. In view of this, we have also demonstrated, both theoretically and experimentally, the SHG of vector light based on the Sagnac scheme with a thin type-I crystal, as well as a long type-0 crystal [37,38].

Notably, despite these works realized the SHG of vector light, compared with the input signal, the SOC state of the output SHG was also transformed. The transformation rule of the SOC state depends on the SoP reference frame of both the input signal and the converting apparatus [37]. However, for vector light (or photons) carrying classical (or quantum) information, the fundamental requirement for upconversion is that the apparatus does not disturb the other DoFs of the signals, especially for the SOC states. To address this issue, a SoP-independent frequency converter that can work for light with arbitrary SoPs (including vector cases) is necessary. In this work, we report SoP-independent upconversion of vector light using a polarization Sagnac nonlinear interferometer based on type-II SHG. Special attention is given to the fidelity of the converting apparatus, specifically, analyzing and comparing the SOC states of the input signals and the corresponding output SHG.

* zhuzhihan@hrbust.edu.cn

Methods and Results. — General vector light can be regarded as a non-separable superposition with respect to a pair of orthogonal SoPs $\hat{\mathbf{e}}_{\pm}$ and associated SoP-dependent spatial modes. Here, without a loss of generality, both in theoretical analysis and experimental demonstration, we choose pairs of conjugate Laguerre-Gaussian (LG) modes as the SoP-dependent spatial modes; given by $LG_{\pm\ell}^p(r, \varphi, z) = u_{|\ell|}^p(r, \varphi, z) \exp[-i(kz \pm \ell\varphi)]$ in the cylindrical coordinates, where ℓ and p denote the azimuthal and radial (spatial) indices of the LG modes, respectively, and $u_{|\ell|}^p(r, \varphi, z)$ is the envelop of the spatial amplitude. The corresponding vector light can be expressed as:

$$\mathbf{E}(r, \varphi, z) = \sqrt{\alpha} LG_{+\ell}^p(r, \varphi, z) \hat{\mathbf{e}}_+ + e^{i\theta} \sqrt{1-\alpha} LG_{-\ell}^p(r, \varphi, z) \hat{\mathbf{e}}_-, \quad (1)$$

where $\alpha \in [0, 1]$ and θ are the weight coefficient and intermodal phase, respectively. It should be noted that $LG_{\pm\ell}^p(r, \varphi, z)$ carry the opposite orbital angular momentum (OAM), i.e., $\pm\ell\hbar$ per photon, but have the same order number of spatial DoF, given by $N = 2p + |\ell|$ [39]. This indicates that each pair of conjugate LG modes spans a spin-like SU(2) space with a mode order of N . In particular, Ref. 40 showed that the corresponding geometric description can be regarded as an OAM equivalent of the SoP Poincaré sphere as $N = 1$. Based on this viewpoint, for a superposed mode consisting of $LG_{\pm\ell}^p(r, \varphi, z)$, the spatial amplitude is invariant upon paraxial propagation, given by $u_{|\ell|}^p(r, \varphi, z) e^{-ikz} [\sqrt{\alpha} e^{-i\ell\varphi} + e^{i\theta} \sqrt{1-\alpha} e^{i\ell\varphi}]$. Thus, we can reformulate Eq. (1) into

$$\begin{aligned} \mathbf{E}^\omega(r, \varphi, z) &= u_{|\ell|}^p(r, \varphi, z) \exp[-ik(\omega)z] \hat{\mathbf{e}}_{\text{SOC}} \\ \hat{\mathbf{e}}_{\text{SOC}} &= \sqrt{\alpha} \exp(-i\ell\varphi) \hat{\mathbf{e}}_+ + e^{i\theta} \sqrt{1-\alpha} \exp(i\ell\varphi) \hat{\mathbf{e}}_-, \end{aligned} \quad (2)$$

where $k(\omega)$ is the angular frequency, and $\hat{\mathbf{e}}_{\text{SOC}}$ denotes the SOC state describing spatially-variant SoPs. The results mean that: first, the vector profiles obeying Eq. (2) are cylindrically symmetric and propagation invariant, and therefore, the corresponding vector light are known as cylindrical vector (CV) modes [41]; second, for CV modes, the SoP profile, governed by $\hat{\mathbf{e}}_{\text{SOC}}$, is independent of the amplitude envelop $u_{|\ell|}^p(r, \varphi, z)$. In addition, for a given $\hat{\mathbf{e}}_{\pm}$ and the associated LG pair, all possible SOC states form a hybrid SU(2) space that can also be visualized as positions on a unit sphere, i.e., the so-called higher-order Poincaré sphere (HOPS) introduced by G. Milione *et al.* [42].

The straightforward description for SoP-independent upconversion is: *to convert the frequency of arbitrary vector light without changing its vector profile and position on the HOPS*. To realize this, we employed a SU(2) nonlinear interferometer based on the polarization Sagnac scheme with a type-II long crystal. Figure 1 shows a schematic of the apparatus, where the vector light is input from port-1 as the signal, the pump input from port-2, and the frequency converted signal (or SHG) is output from port-3. The input signal was first split using a dual-wavelength polarizing beam splitter (d -PBS), and if we define $\hat{\mathbf{e}}_+ = \sqrt{\beta} \hat{\mathbf{e}}_H + e^{i\theta} \sqrt{1-\beta} \hat{\mathbf{e}}_V$ and $\hat{\mathbf{e}}_- = \sqrt{1-\beta} \hat{\mathbf{e}}_H - e^{i\theta} \sqrt{\beta} \hat{\mathbf{e}}_V$, the signal in the interferometer can be represented as:

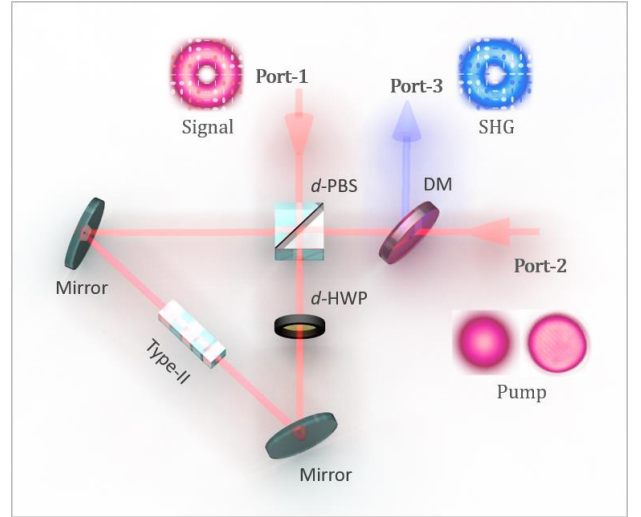


FIG. 1. Schematic of the polarization Sagnac nonlinear interferometer. The key components include the *dual-wavelength* polarizing beam splitter (d -PBS), *dual-wavelength* half-wave plate (d -HWP), and dichroic mirror (DM).

$$\mathbf{E}^\omega(r, \varphi, z) = E_H^\omega(r, \varphi, z) \hat{\mathbf{e}}_H + e^{i\theta} E_V^\omega(r, \varphi, z) \hat{\mathbf{e}}_V, \quad (3)$$

where $E_H^\omega(r, \varphi, z)$ and $E_V^\omega(r, \varphi, z)$ are two SoP-dependent spatial modes, with respect to $\hat{\mathbf{e}}_H$ and $\hat{\mathbf{e}}_V$, that propagate clockwise and anticlockwise in the Sagnac loop, respectively, see Appendix A for details. At port-2, a diagonal-polarized pump, given by $E_p^\omega(r, \varphi, z) \hat{\mathbf{e}}_D$, enters the loop with a transmission-reflection ratio of 50:50, where a Gaussian ($LG_0^0(r, \varphi, z)$) or flat-top beam ($FT(r, z) = \exp[-ik(\omega)z]$) is employed as required as the pump. It should be noted that the Gaussian pump only works for the signal without a radial index (i.e., $p=0$), because the coupled spatial amplitude, $u_0^0(r, \varphi, z) * u_{|\ell|}^p(r, \varphi, z)$, is still a LG mode but this does not hold for $p \neq 0$ [43,44]. In the Sagnac loop, the presence of a dual-wavelength half wave plate (d -HWP) leads to a SoP swapping between $\hat{\mathbf{e}}_H$ and $\hat{\mathbf{e}}_V$ for any beams passing it, including pump, signal and SHG. In consequence, two type-II SHG processes [21], i.e., $E_H^\omega \hat{\mathbf{e}}_V * E_p^\omega \hat{\mathbf{e}}_H \rightarrow E_H^{2\omega}(r, \varphi, z) \hat{\mathbf{e}}_H$ and $E_V^\omega \hat{\mathbf{e}}_H * E_p^\omega \hat{\mathbf{e}}_H \rightarrow E_V^{2\omega}(r, \varphi, z) \hat{\mathbf{e}}_V$, occur for clockwise and anticlockwise trips of the signal beam, respectively. Then, the two generated scalar SHG with $\hat{\mathbf{e}}_H$ and $\hat{\mathbf{e}}_V$, respectively, overlap on the d -PBS again and output from a dichroic mirror (DM). Because of the phase-locking structure of the apparatus (because the fact of all beams propagating along the same loop), the intramodal phase $e^{i\theta}$ is maintained for the whole transformation. As a result, the SHG light appearing from port-3 is $\mathbf{E}^{2\omega}(r, \varphi, z) = E_H^{2\omega}(r, \varphi, z) \hat{\mathbf{e}}_H + e^{i\theta} E_V^{2\omega}(r, \varphi, z) \hat{\mathbf{e}}_V$, i.e., a SoP-independent upconversion $\mathbf{E}^\omega(r, \varphi, z) \rightarrow \mathbf{E}^{2\omega}(r, \varphi, z)$ is achieved.

Figure 2 shows a schematic of the experimental setup, where a continuous laser at 800 nm (Toptica TA pro) was used as the fundamental frequency light for the SHG. The laser output from a single-mode fiber collimator was first converted into a perfect TEM₀₀ mode by passing through a spatial filter.

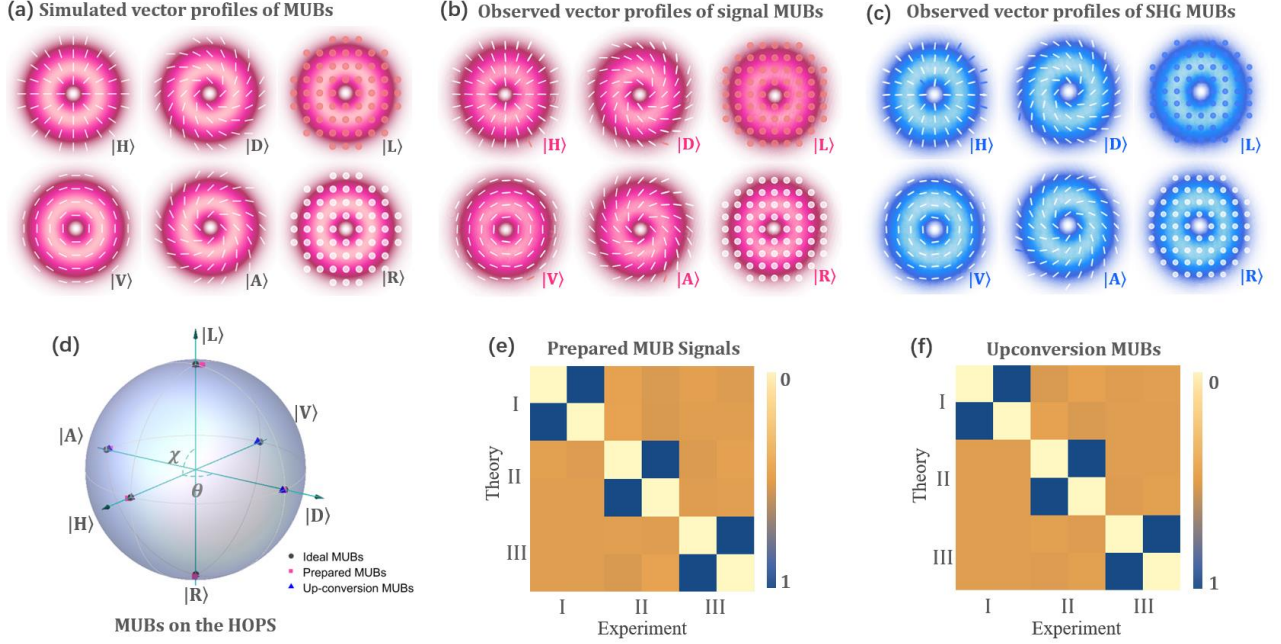


FIG. 3. SoP-independent upconversion for complete MUBs of the HOPS spanned by $|L\rangle = |\hat{\mathbf{e}}_L, +1\rangle$ and $|R\rangle = |\hat{\mathbf{e}}_R, -1\rangle$, where (a)–(c) are vectorial profiles of the simulated MUBs, prepared signals and the corresponding SHG, respectively. (d) Positions of the MUBs on the HOPS. (e) and (f) Experimental correlation matrix for different MUBs obtained from the prepared signals and the corresponding SHG, respectively.

we also performed complete MUB projections for them, and the corresponding correlation matrices for the signals and SHG outputs are shown in Figs. 3(e) and (f), respectively. These results verify the ability of the frequency conversion of the vector light with a rotationally invariant SOC structure. Moreover, an additional result for the MUBs with $\ell=2$ is provided in Appendix B.

Next, we demonstrate SoP-independent upconversion for CV modes based on arbitrary SoP with vector profiles are no longer rotationally invariant. For this, we consider SOC states on two specific HOPSs, given by:

$$\begin{aligned} & \sqrt{\alpha} \exp(-i\varphi) \hat{\mathbf{e}}_H + e^{i\theta} \sqrt{1-\alpha} \exp(i\varphi) \hat{\mathbf{e}}_V \\ & \sqrt{\alpha} \exp(-i2\varphi) \hat{\mathbf{e}}_D + e^{i\theta} \sqrt{1-\alpha} \exp(i2\varphi) \hat{\mathbf{e}}_A, \end{aligned} \quad (5)$$

where four states were chosen for each sphere, as shown by the gray points plotted on the HOPSs in Figs. 4(a) and (c). The experimental results, i.e., the positions of the experimentally prepared signals and the associated SHG output obtained via spatial Stokes measurement, are shown by the red and blue points, respectively, in Figs. 4(a) and (c). For both spheres, we see that each group of three points with different colors are in high proximity, indicating high accuracy for the signal preparation as well as the high fidelity of the upconversion. For a more intuitive display of the results, Figs. 4(b) and (d) show the vector profiles of the SOC states on the two spheres, including the theoretical expectations, observed signals, and corresponding SHG output. We see that all the observations for the signal and SHG are once again in excellent agreement with each other, as well as with the theoretically expected

results. Additionally, a calculated SOC state fidelity based on the results is provided in Appendix B.

In above experiments, the SoP independence of the upconversion was true for CV modes without the radial index, and all the SHG output were pumped by a Gaussian beam. From Eq. (2), it can be seen that to maintain the vector profile (or SOC structure) of a CV mode with $p=0$, using an easy-to-obtain Gaussian beam as the pump is sufficient. This is because the amplitude envelopes of the nonlinear polarizations (NP) excited by a beating field $u_0^0(r, \varphi, z) * u_{|l|}^0(r, \varphi, z)$ in the crystal still has an LG distribution. This particular result, however, is no longer true for the general case $p \neq 0$. To demonstrate this, we consider a “radial polarized” signal with $p=2$, given by $\sqrt{1/2}[LG_{+1}^2(r, \varphi, z) \hat{\mathbf{e}}_L + e^{i\theta} LG_{-1}^2(r, \varphi, z) \hat{\mathbf{e}}_R]$. Figures 5(a) and (b) show the upconversion of this signal pumped using a Gaussian beam. We see that, while its azimuthal-variant SoP is maintained in the upconversion, the radial intensity profile was destroyed and is no longer propagation invariant. Additionally, our simulations have excellent agreement with the experimental observation; for this, in Ref. 44 we provide a general theory for the transformation of the radial mode of the LG beam in upconversion. To overcome this distortion, using a flattop beam as the pump is necessary, which can be easily obtained with high efficiency (~90% efficiency using a Holoeye PLUTO-2-NIR-080) via a phase-only light shaping technique [45]. Figures 5(c) and (d) show the upconversion pumped by a flattop beam, where we see that the radial amplitude of the SHG output agrees well with that of the signal for both near and far fields.

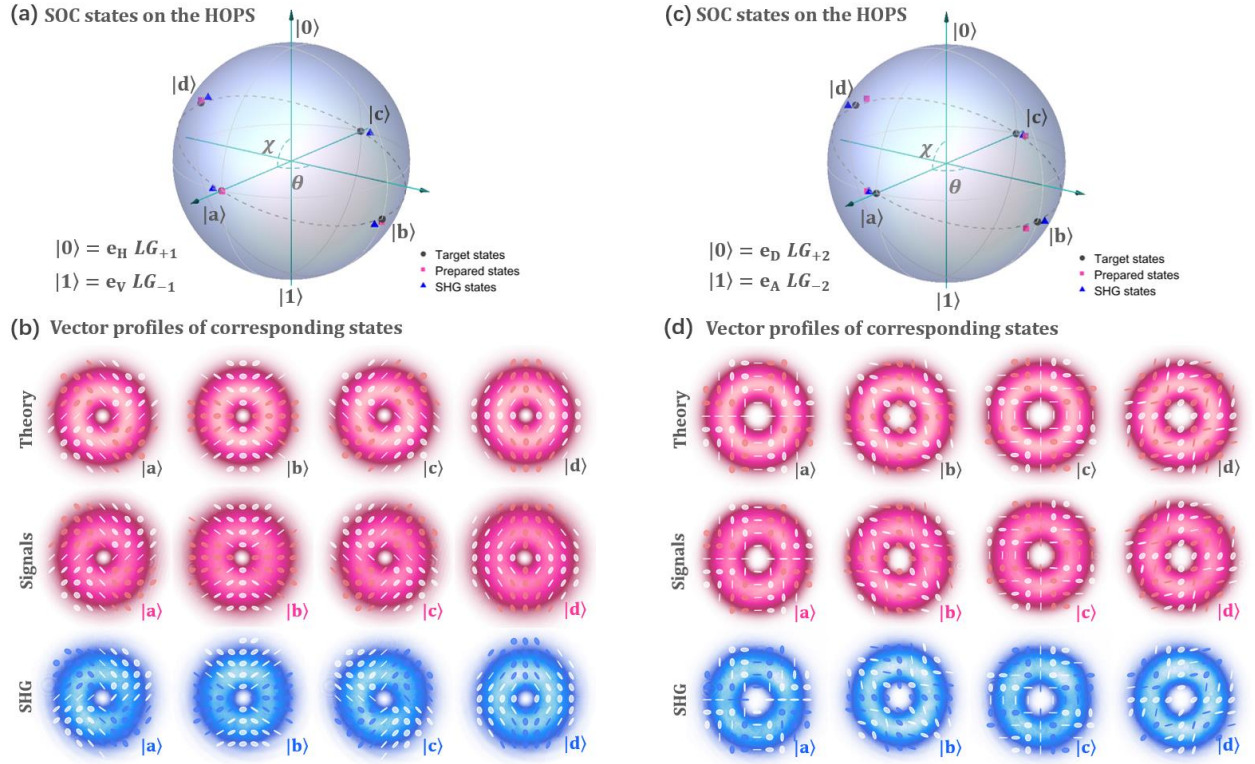


FIG. 4. SoP-independent upconversion for the SOC states defined by an arbitrary SoP basis. (a) SOC states on the HOPS defined by $|0\rangle = |\hat{e}_H, +1\rangle$ and $|1\rangle = |\hat{e}_V, -1\rangle$, and (b) vector profiles of the corresponding states. (c) SOC states on the HOPS defined by $|0\rangle = |\hat{e}_D, +2\rangle$ and $|1\rangle = |\hat{e}_A, -2\rangle$, and (d) vector profiles of the corresponding states.

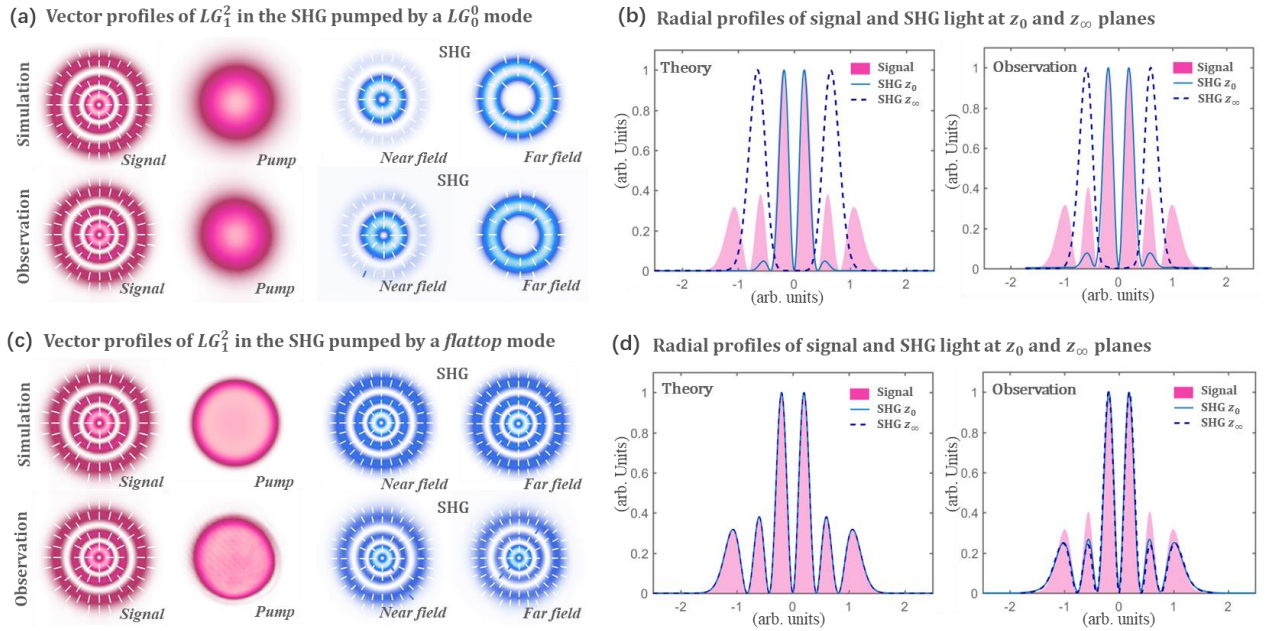


FIG. 5. SoP-independent upconversion for the SOC states carrying radial structures. (a) Simulated and observed vector profiles of the SHG of LG_1^2 pumped by a Gaussian mode, and (b) comparison of the corresponding radial profiles obtained by simulation and observation. (c) Simulated and observed vector profiles of the SHG of LG_1^2 pumped by a flattop beam, and (d) comparison of the corresponding radial profiles obtained by simulation and observation.

Discussion and conclusion. — It should be noted that full SoP independence can be classified into two DoFs, i.e., radial and azimuthal, and we shortly review the key to realize this independence. First, for the apparatus, any input signal carrying vector SoP in the interferometer is identified as $E_H^\omega(r, \varphi, z)\hat{\mathbf{e}}_H + e^{i\phi}E_V^\omega(r, \varphi, z)\hat{\mathbf{e}}_V$. Second, a flattop pump can exactly convert two SoP-dependent spatial modes, i.e., $E_H^\omega(r, \varphi, z)$ and $E_V^\omega(r, \varphi, z)$. Finally, the common-path loop can stably transfer the intramodal phase $e^{i\phi}$ to the final SHG output. However, as demonstrated above, except for the CV modes with $p=0$, for general vector light such as CV modes with $p \neq 0$ or the well-known full Poincaré modes [48], a flattop pump that can realize a spatial-mode-independent upconversion is necessary. Based on this principle, a recent work demonstrated azimuthal-index independent sum-frequency generation for the upconversion of high-dimension quantum states [49]. Additionally, for exploring the full quantum resource of the spatial-mode DoF, the radial indices of LG modes have recently gained a considerable research interest [50-53]. Within this perspective, the principle we demonstrated here provides a feasible way to realize a vector full-field quantum frequency converter.

In summary, in this proof-of-principle work, we demonstrated SoP-independent upconversion for vector light. The apparatus was based on a polarization Sagnac nonlinear interferometer with a type-II PPKTP crystal, where a flattop beam (or Gaussian beam in particular cases) with a variable beam size was employed as the pump. Our results show that the vector profile and the associated SOC state of the signal light can be safely transferred into the SHG output with a high fidelity. The principle demonstrated here lays the foundation for SoP-independent high-dimension quantum frequency conversion, and also pave the way for realization of upconversion detection for SoP-resolved polarization imaging and microscopy [50-53].

ACKNOWLEDGMENT

This work was supported by the National Natural Science Foundation of China (Grant Nos. 11934013 and 61975047).

Appendix A

According to the relation $\hat{\mathbf{e}}_+ = \sqrt{\beta}\hat{\mathbf{e}}_H + e^{i\phi}\sqrt{1-\beta}\hat{\mathbf{e}}_V$ and $\hat{\mathbf{e}}_- = \sqrt{1-\beta}\hat{\mathbf{e}}_H - e^{i\phi}\sqrt{\beta}\hat{\mathbf{e}}_V$, two SoP-dependent spatial modes in Eq. (3) is given by

$$\begin{aligned} E_H^\omega(r, \varphi, z) &= u_r^p(r, \varphi, z)\exp[-ik(\omega)z] \\ &\times \left[\sqrt{\alpha\beta}\exp(-i\ell\varphi) + e^{i\theta}\sqrt{(1-\alpha)(1-\beta)}\exp(i\ell\varphi) \right] \\ E_V^\omega(r, \varphi, z) &= u_r^p(r, \varphi, z)\exp[-ik(\omega)z] \\ &\times \left[\sqrt{(1-\alpha)\beta}\exp(-i\ell\varphi) - e^{i\theta}\sqrt{\alpha(1-\beta)}\exp(i\ell\varphi) \right]. \end{aligned} \quad (6)$$

Now we consider the special case of $p=0$. For a Gaussian pump, i.e., $LG_0^0(r, \varphi, z) = u_0^0(r, \varphi, z)\exp[-ik(\omega)z]$, the excited NP of SHG in the clockwise and anticlockwise directions are given by

$$\begin{aligned} \mathbf{P}_{clock}^{NL} &\propto LG_0^0(r, \varphi, z_0)E_H^\omega(r, \varphi, z_0) \\ &= u_0^0(r, \varphi, z_0)u_r^0(r, \varphi, z_0)\exp[-ik(2\omega)z] \\ &\times \left[\sqrt{\alpha\beta}\exp(-i\ell\varphi) + e^{i\theta}\sqrt{(1-\alpha)(1-\beta)}\exp(i\ell\varphi) \right] \\ \mathbf{P}_{anticlock}^{NL} &\propto LG_0^0(r, \varphi, z_0)E_V^\omega(r, \varphi, z_0) \\ &= u_0^0(r, \varphi, z_0)u_r^0(r, \varphi, z_0)\exp[-ik(2\omega)z] \\ &\times \left[\sqrt{(1-\alpha)\beta}\exp(-i\ell\varphi) - e^{i\theta}\sqrt{\alpha(1-\beta)}\exp(i\ell\varphi) \right]. \end{aligned} \quad (7)$$

Note, due to $u_0^0(r, \varphi, z_0)u_r^0(r, \varphi, z_0) \propto u_r^0(r, \varphi, z_0)$, thus we have $\mathbf{P}_{clock}^{NL} \propto E_H^{2\omega}(r, \varphi, z)$ and $\mathbf{P}_{anticlock}^{NL} \propto E_V^{2\omega}(r, \varphi, z)$, indicating a transformation of $\mathbf{E}^\omega(r, \varphi, z) \rightarrow \mathbf{E}^{2\omega}(r, \varphi, z)$ is achieved.

Appendix B

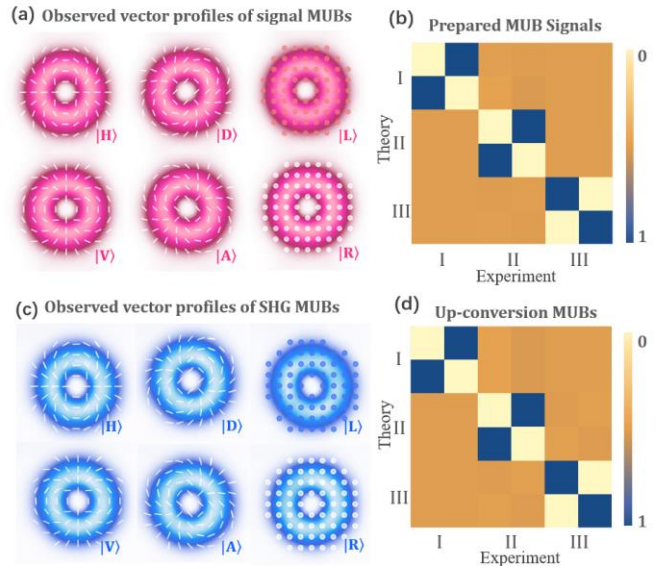


FIG. 6. Additional results for complete MUBs of the HOPS spanned by $|L\rangle = |\hat{\mathbf{e}}_z, +2\rangle$ and $|R\rangle = |\hat{\mathbf{e}}_z, -1\rangle$, where (a) and (b) are observed vectorial profiles of the signals and the corresponding correlation matrix, respectively; (c) and (d) are observed vectorial profiles of the SHG and the corresponding MUB correlation matrix, respectively.

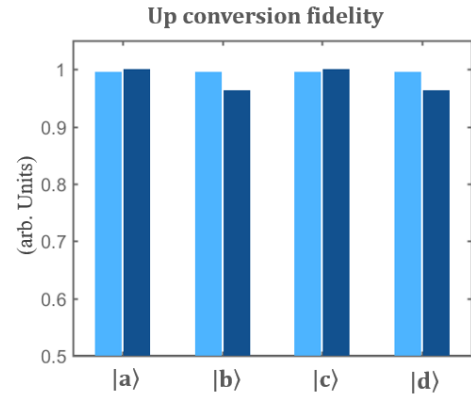


FIG. 7. Upconversion fidelity obtained from the inner products of the signals and their corresponding SHG, where light and dark blue corresponds to data in Fig. 4 (a) and (b), respectively.

References

1. J. Chen, C.-H Wan, and Q.-W. Zhan. Vectorial optical fields: recent advances and future prospects. *Sci. Bull.* **63**, 54 (2018).
2. C. Rosales-Guzmán, B. Ndagano and A. Forbes. A review of complex vector light fields and their applications. *J. Opt.* **20**, 123001 (2018).
3. H. Rubinsztein-Dunlop, *et al.* Roadmap on structured light. *J. Opt.* **19**, 013001 (2017).
4. K. Y. Bliokh, F. J. Rodriguez-Fortuno, F. Nori, *et al.* Spin-orbit interactions of light. *Nat. Photon.* **9**, 796, (2015).
5. F. Cardano, L. Marrucci. Spin-orbit photonics. *Nat. Photon.* **9**, 776 (2015).
6. P. Chen, *et al.* Liquid-Crystal-Mediated Geometric Phase: From transmissive to Broadband Reflective Planar Optics. *Adv. Mater.* 1903665 (2019)
7. D. Pohl, Operation of a Ruby laser in the purely transverse electric mode TE₀₁. *Appl. Phys. Lett.* **20**, 266–267 (1972).
8. Y. Mushiake, K. Matzumura, and N. Nakajima, Generation of radially polarized optical beam mode by laser oscillation. *Proc. IEEE* **60**, 1107 (1972).
9. S. Quabis, R. Dorn, M. Eberler, O. Glöckl, and G. Leuchs. Focusing light into a tighter spot. *Opt. Commun.* **179**, 1–7 (2000).
10. R. Dorn, S. Quabis, and G. Leuchs. Sharper focus for a radially polarized light beam. *Phys. Rev. Lett.* **91**, 233901 (2003).
11. P. Török and P. Munro, “The use of Gauss–Laguerre vector beams in STED microscopy,” *Opt. Express* **12**, 3605–3617 (2004).
12. R. Chen, K. Agarwal, C. J. R. Sheppard, and X. Chen, Imaging using cylindrical vector beams in a high-numerical-aperture microscopy system. *Optics Lett.* **38**, 3111-4 (2013).
13. C. V. S. Borges, M. Hor-Meyll, J. A. O. Huguenin, and A. Z. Khoury. Bell-like inequality for the spin-orbit separability of a laser beam. *Phys. Rev. A* **82**, 033833 (2010).
14. V. D’Ambrosio, *et al.* Complete experimental toolbox for alignment-free quantum communication. *Nat. Commun.* **3**:961 (2012).
15. G. Vallone, *et al.* Free-Space Quantum Key Distribution by Rotation-Invariant Twisted Photons, *Phys. Rev. Lett.* **113**, 060503 (2014).
16. V. D’Ambrosio, *et al.* Entangled vector vortex beams. *Phys. Rev. A* **94**, 030304(R) (2016).
17. S. Berg-Johansen, F. Töppel, B. Stiller, P. Banzer, M. Ornigotti, E. Giacobino, G. Leuchs, A. Aiello, and C. Marquardt, Classically entangled optical beams for high-speed kinematic sensing. *Optica* **2**, 864-868 (2015).
18. S. Slussarenko, A. Alberucci, C. P. Jisha, B. Piccirillo, E. Santamato, G. Assanto, L. Marrucci. Guiding light via geometric phases. *Nat. Photon.* **10**, 571-575 (2016).
19. L. Marrucci, E. Karimi, S. Slussarenko *et al.*, Spin-to-orbital conversion of the angular momentum of light and its classical and quantum applications, *J. Opt.* **13**, 064001 (2011).
20. L. Zhang, X. Qiu, F. Li, H. Liu, X. Chen, and L. Chen. Second harmonic generation with full Poincaré beams. *Opt. Express*, **26**(9), 11678 (2018).
21. H.-J. Wu, H.-R. Yang, C. Rosales-Guzmán, W. Gao, B.-S. Shi, and Z.-H. Zhu. Vectorial nonlinear optics: Type-II second-harmonic generation driven by spin-orbit-coupled fields. *Phys. Rev. A* **100**, 053840 (2019).
22. L. J. Pereira, W. T. Buono, D. S. Tasca, K. Dechoum, and A. Z. Khoury. Orbital-angular-momentum mixing in type-II second-harmonic generation. *Phys. Rev. A* **96**, 053856 (2017).
23. Stanislovaitytė, P., Matijošius, A., Šetkus, V., & Smilgevičius, V. Peculiarities of second harmonic generation by paraxial beams with radial/azimuthal polarization in type II nonlinear crystal. *Lithuanian Journal of Physics*, **54**(3) (2014).
24. Gu, B., Cao, X., Rui, G., & Cui, Y. Vector beams excited nonlinear optical effects. *Journal of Nonlinear Optical Physics & Materials*, **27**(04), 1850045 (2018).
25. Kozawa, Y., and Sato, S. Observation of the longitudinal field of a focused laser beam by second-harmonic generation. *J. Opt. Soc. Am. B.* **25**(2), 175-179 (2008).
26. J. Vieira, R. M. G. M. Trines, E. P. Alves, R. A. Fonseca, J. T. Mendonça, R. Bingham, P. Norreys, and L. O. Silva. Amplification and generation of ultra-intense twisted laser pulses via stimulated Raman scattering. *Nat. Commun.* **7**, 10371 (2016).
27. Bouchard, F., Larocque, H., Yao, A. M., Travis, C., DeLeon, I., Rubano, A., Karimi, E., Oppo, G. L., Boyd, R. W. Polarization Shaping for Control of Nonlinear Propagation. *Phys. Rev. Lett.* **117**, 233903 (2016).
28. Z.-H. Zhu, P. Chen, L.-W. Sheng, Y.-L. Wang, W. Hu, Y.-Q. Lu, and W. Gao, Generation of strong cylindrical vector pulses via stimulated Brillouin amplification. *Appl. Phys. Lett.* **110**, 141104 (2017).
29. F. Kong, C. Zhang, H. Larocque, F. Bouchard, Z. Li, M. Taucer, G. Brown, S. Severino, T. J. Hammond, E. Karimi, and P. B. Corkum. Spin-constrained orbital-angular-momentum control in high-harmonic generation. *Phys. Rev. Research* **1**(3), 032008, (2019).
30. F. Kong, H. Larocque, E. Karimi, P.B. Corkum, C. Zhang. Generating few-cycle radially polarized pulses. *Optica* **6**(2), 160-164, (2019).
31. M. V. Chekhova and Z. Y. Ou, Nonlinear interferometers in quantum optics. *Adv. Opt. Photon.* **8**, 104 (2016)
32. P. G. Kwiat, E. Waks, A. G. White, I. Appelbaum, and P. H. Eberhard, Ultrabright source of polarization-entangled photons. *Phys. Rev. A* **60**, R773 – R776 (1999).
33. B.-S. Shi and A. Tomita. Generation of a pulsed polarization entangled photon pair using a Sagnac interferometer. *Phys. Rev. A* **69**, 013803 (2004).
34. T. Kim, M. Fiorentino, and F. N. C. Wong. Phase-stable source of polarization-entangled photons using a polarization Sagnac interferometer. *Phys. Rev. A* **73**, 012316 (2006).
35. H. Liu, H. Li, Y. Zheng, and X. Chen, Nonlinear frequency conversion and manipulation of vector beams. *Opt. Lett.* **43**, 5981-5984 (2018).
36. R. K. Saripalli, A. Ghosh, A. Chaitanya, and G. K. Samanta. Frequency-conversion of vector vortex beams with space-variant polarization in single-pass geometry. *Appl. Phys. Lett.* **115**, 051101 (2019).
37. H.-J. Wu, Z.-Y. Zhou, W. Gao, B.-S. Shi, and Z.-H. Zhu. Dynamic tomography of the spin-orbit coupling in nonlinear optics. *Phys. Rev. A* **99**, 023830 (2019).
38. C. Yang, Z.-Y. ZHOU, Y. Li, Y.-H. Li, S.-L. Liu, S.-K. Liu, Z.-H. Xu, G.-C. Guo, and B.-S. Shi. Nonlinear frequency conversion and manipulation of vector beams in a Sagnac loop. *Opt. Lett.* **44**, 219-222 (2019).
39. L. Allen, J. Courtial, and M. J. Padgett. Matrix formulation for the propagation of light beams with orbital and spin angular momenta. *Phys. Rev. E* **60**, 7497 (1999).
40. M. J. Padgett and J. Courtial. Poincaré-sphere equivalent for light beams containing orbital angular momentum. *Opt. Lett.* **24**, 430 (1998).
41. Zhan Q. Cylindrical vector beams: from mathematical concepts to applications. *Adv. Opt. Photon.* **1**,1 (2009).
42. G. Milione, H. I. Sztul, D. A. Nolan, and R. R. Alfano, Higher-Order Poincaré Sphere, Stokes Parameters, and the Angular Momentum of Light. *Phys. Rev. Lett.* **107**, 053601 (2011).
43. J. Courtial, K. Dholakia, L. Allen, and M. J. Padgett. Second-harmonic generation and the conservation of orbital angular

- momentum with high-order Laguerre-Gaussian modes. *Phys. Rev. A* **56**, 4193 (1997).
44. H.-J. Wu, L.-W. Mao, Y.-J. Yang, C. Rosales-Guzmán, W. Gao, B.-S. Shi, Z.-H. Zhu. Radial modal transition of Laguerre-Gauss modes in second-harmonic generation. [arXiv:1912.05585](#).
 45. C. Rosales-Guzmán, and A. Forbes. *How to Shape Light with Spatial Light Modulators*. (SPIE Press Book, 2017).
 46. B.-S. Yu, H.-J. Wu, H.-R. Yang, W. Gao, C. Rosales-Guzman, B.-S. Shi, Z.-H. Zhu. Full characterization of spin-orbit coupled photons via spatial-Stokes measurement. [arXiv:1907.04035](#).
 47. G. Vallone, et al. Free-Space Quantum Key Distribution by Rotation-Invariant Twisted Photons, *Phys. Rev. Lett.* **113**, 060503 (2014).
 48. A. M. Beckley, T. G. Brown, and M. A. Alonso, Full Poincaré beams, *Opt. Express* **18**, 10777 (2010).
 49. S.-L. Liu, C. Yang, Z.-H. Xu, *et al.* High-dimensional quantum frequency converter. *Phys. Rev. A* **101**, 012339 (2020).
 50. V. D. Salakhutdinov, E. R. Eliel, and W. Löffler. Full-Field Quantum Correlations of Spatially Entangled Photons. *Phys. Rev. Lett.* **108**, 173604 (2012).
 51. D. Geelen and W. Löffler. Walsh modes and radial quantum correlations of spatially entangled photons. *Opt. Lett.* **38**, 4108-4111 (2013).
 52. X. Gu, M. Krenn, M. Erhard, and A. Zeilinger, Gouy Phase Radial Mode Sorter for Light: Concepts and Experiments, *Phys. Rev. Lett.* **120**, 103601 (2018).
 53. Lixiang Chen, Tianlong Ma, Xiaodong Qiu, Dongkai Zhang, Wuhong Zhang, and Robert W. Boyd. Realization of the Einstein-Podolsky-Rosen Paradox Using Radial Position and Radial Momentum Variables. *Phys. Rev. Lett.* **123**, 060403 (2019).
 54. A. Barh, P. J. Rodrigo, L. Meng, C Pedersen, and P. Tidemand-Lichtenberg. Parametric upconversion imaging and its applications. *Adv. Opt. Photon.*, **11**(4): 952-1019 (2019).
 55. X. Qiu, F. Li, W. Zhang, Z. Zhu, and L. Chen. Spiral phase contrast imaging in nonlinear optics: seeing phase objects using invisible illumination. *Optica* **5**(2), 208-212 (2018).